Atmospheric
Chemistry
and Physics

The strengthening relationship between Eurasian snow cover and December haze days in central North China after the mid-1990s

Zhicong Yin[1,2] **and Huijun Wang**[1,2]

[1]Key Laboratory of Meteorological Disaster, Ministry of Education/Joint International Research Laboratory of Climate and Environment Change (ILCEC)/Collaborative Innovation Center on Forecast and Evaluation of Meteorological Disasters (CIC-FEMD), Nanjing University of Information Science & Technology, Nanjing 210044, China TS1
[2]Nansen-Zhu International Research Centre, Institute of Atmospheric Physics, Chinese Academy of Sciences, Beijing, China

Correspondence: Zhicong Yin (yinzhc@163.com)

Abstract. TS2 TS3 The haze pollution in December has become increasingly serious over recent decades and imposes damage on society, ecosystems, and human health. In addition to anthropogenic emissions, climate change and variability were conducive to haze in China. In this study, the relationship between the snow cover over eastern Europe and western Siberia (SC_{ES}) and the number of haze days in December in central North China CE1 was analyzed. This relationship significantly strengthened after the mid-1990s, which is attributed to the effective connections between the SC_{ES} and the Eurasian atmospheric circulations. During 1998–2016, the SC_{ES} significantly influenced the soil moisture and land surface radiation, and then the combined underlying drivers of enhanced soil moisture and radiative cooling moved the the East Asia jet stream northward and induced anomalous, anti-cyclonic circulation over central North China. Modulated by such atmospheric circulations, the local lower boundary layer, the decreased surface wind, and the more humid air were conducive to the worsening dispersion conditions and frequent haze occurrences. In contrast, from 1979 to 1997, the linkage between the SC_{ES} and soil moisture was negligible. Furthermore, the correlated radiative cooling was distributed narrowly and far from the key area of snow cover. The associated atmospheric circulations with the SC_{ES} were not significantly linked with the ventilation conditions over central North China. Consequently, the relationship between the SC_{ES} and the number of hazy days in central North China was insignificant before the mid-1990s but has strengthened and has become significant since then.

1 Introduction

In December 2016, central North China (CNC, located at 30–41° N, 110–120° E), where more than 300 million people live, experienced severe haze pollution (Yuan and Ma, 2017). On 70 % of the days in December 2016, the people who lived in CNC breathed polluted air, which influenced the health of everyone, especially children. Beyond anthropogenic emissions, the atmospheric circulations (Yin and Wang, 2017) and aerosol–meteorology feedback (Ding et al., 2016; Yang et al., 2017a) have significantly contributed the severe haze in China. Many recent previous studies have documented that climate change and variability contributed to the severe winter haze pollution in China (Cai et al., 2017; Ding and Liu, 2014; Wang and Chen, 2016; Yang TS4 et al., 2016). For the long-term trend of haze pollution, Wang and Chen (2016 TS5) illustrated the roles of climate change in eastern China and emphasized the effects of the Arctic sea ice. Cai et al. (2017) analyzed the weather conditions conductive to severe haze in Beijing that is more frequent under climate change CE2. There were also previous studies on the interannual variation in haze and associated climatic conditions. The possible physical processes in the atmosphere that caused the haze events may have included (i) when the positive pattern of eastern Atlantic/western Russia CE3 and western Pacific (Yin et al., 2017) occurred together or partly and (ii) the anomalous anti-cyclone over CNC and the Japan Sea would be enhanced and then confined the vertical motion of atmospheric matters CE4. Furthermore, the southerly anomalies that are characteristic of East Asian winter monsoons (Li et al., 2015; Yin et al., 2015) may have weakened the cold

air and wind speed but enhanced the transportation of humid air flow and aerosols (Yang et al., 2017b). Thus, the vertical and horizontal dispersion capacities were both restricted, which resulted in haze pollution. Concerning external mechanisms, the investigated climatic factors include sea surface temperature (SST) over the subtropical western Pacific (Yin and Wang, 2016; Gao and Chen, 2017), Arctic sea ice (Wang and Chen, 2015, TS6 2016) and the topography of the Tibetan Plateau (Xu et al., 2016). In addition, the large-scale SST patterns, such as the El Niño-Southern Oscillation and the Pacific Decadal Oscillation, also showed close relationships with the haze pollution in the east of China (Gao et al. TS7, 2015).

Unlike the declining trend of Arctic sea ice, Eurasian snow cover has been increasing over the last two decades (Cohen et al., 2012), probably due to the increased southward moisture transport from the melted Arctic Ocean (Deser et al., 2010). The anomalous snow cover influenced the exchange of heat and moisture in atmosphere–land interactions, which were characterized by high albedo and water effects (Chen et al., 2012 TS8). Starting in autumn, the snow cover over Eurasia began to accumulate gradually and was significantly correlated with the winter climate in the Northern Hemisphere (Foster et al., 1983; Zhang et al., 2007; Li and Wang, 2014; Li et al., 2017; Xu et al., 2017). In October, enhanced snow cover was associated with a negative Arctic Oscillation phase (Gong et al., 2007) via the stratosphere–troposphere coupled planetary wave activity (Cohen et al., 2007). The change in the October–November (ON) Eurasian snow cover was also considered as a primary factor for the recent recovery of the Siberian High intensity over the last few decades (Jeong et al., 2011). Furthermore, there was a significant negative correlation between the October snow cover located in eastern Siberia and in the area northeast of Lake Baikal and the following winter air temperature over Northeast China (Li et al., 2017). A notable feature related with the impact of snow cover was the change in the relationship with the winter climate in the Northern Hemisphere after the mid-1990s. Both observational evidence and model simulations demonstrated a significant change in the relationship between the autumn Eurasian snow depth and the East Asian winter monsoon (Li and Wang, 2014). Xu et al. (2017) applied a 15-year sliding correlation to show the intensification in the connection between the October snow cover and the January "warm Arctic-cold Eurasia" pattern since the mid-1990s. Specifically investigating the impact of snow cover on December haze days over the CNC area (DHD$_{CNC}$), Yin and Wang (2017) illustrated that DHD$_{CNC}$ significantly related with the ON snow cover over eastern Europe and western Siberia (SC$_{ES}$). Zou et al. (2017) also pointed out that there was a close relationship between Eurasian snow and haze in China based on the observational and numerical analysis. Thus, a question raised here was whether there was a significant change in the connection between SC$_{ES}$ and DHD$_{CNC}$. Motivated by many previous studies, we attempted to answer this question and explored the associated physical mechanisms. The investigation described in this paper will highlight the impact of SC$_{ES}$, recognize the changes in their relationships with other variables, and improve the seasonal prediction potential of the DHD$_{CNC}$.

The remainder of this paper is organized as follows. The data and methods are described in Sect. 2. In Sect. 3, we analyzed the strengthening relationship between SC$_{ES}$ and DHD$_{CNC}$, as well as the associated atmospheric circulations. Then, the possible physical mechanisms were studied in Sect. 4. The main conclusions of this study and necessary discussion material are included in Sect. 5.

2 Datasets and methods

The geopotential height at 500 hPa (Z500) and 200 hPa (Z200), the zonal wind at 200 hPa (U200), the wind at 850 hPa (UV850), the wind speed at the surface, the sea level pressure (SLP), the surface air temperature (SAT), the surface relative humidity, the vertical wind, the surface net longwave radiation, and the surface net shortwave radiation (upward radiation is positive) data were downloaded from the National Center for Environmental Prediction and the National Center for Atmospheric Research. These 2.5° × 2.5° reanalysis datasets were available for the period between 1948 and 2016 (Kalnay et al., 1996). In addition, the 1° × 1° planetary boundary layer height (BLH) was derived from the ERA-Interim dataset (Dee et al., 2011). The monthly snow cover data were supported by the Rutgers University (Robinson et al., 1993). The sub-daily (i.e., 4 times per day) routine meteorological observations (i.e., relative humidity, visibility, wind speed, and weather phenomena) were collected by the National Meteorological Information Center, China Meteorological Administration. According to Yin et al. (2017), the haze data were calculated mainly based on the observed visibility and the relative humidity. Because the interval of the haze data was 6 hours, we defined a haze day as a day with haze occurring at any of the four times. DHD$_{CNC}$ was the mean number of haze days over the CNC area.

3 Strengthening relationship and associated atmospheric circulations

From 1979 to 1997, interannual variation was the main change mode of the DHD$_{CNC}$, and the linear sloped trend was not significant (Figure omitted TS9). Thereafter, the decadal component of the DHD$_{CNC}$ became significant; that is, the haze days decreased from 1998 to 2010 but then increased rapidly (Fig. 1a), reaching more than 21 days in 2016. The minimum number of DHD$_{CNC}$ was 10 days and occurred in 2010, while the maximum (21 days) appeared in 2016 (Yin and Wang, 2017). As illustrated by Yin and Wang (2017), the DHD$_{CNC}$ has a significantly close relationship with SC$_{ES}$ between 1979 and 2016 (Fig. 1b); SC$_{ES}$ was

Please note the remarks at the end of the manuscript.

Figure 2. The CC between the SC_{ES} and snow cover **(a)** from 1979 to 1997 and **(b)** from 1998 to 2016. The black dots indicate that the CC exceeded the 95 % confidence level (*t* test). The black box represents the ES area. The linear trend is removed. The green lines indicate that the interannual variations in snow cover were obvious in this region.

Figure 1. (a) The variation in the normalized DHD_{CNC} (black) and SC_{ES} (blue) from 1979 to 2016 after detrending and the 21-year running correlation coefficient (CC) between the DHD_{NH} and SC_{ES} before (solid, red) and after (dashed, red) detrending. **(b)** The CC between the DHD_{CNC} and snow cover from 1979 to 2016 after detrending. The black dots indicate CCs exceeding the 95 % confidence level (*t* test). The black box represents the ES area. The subscripts "dt" and "OS" in panel **(a)** indicate that the CC was calculated by the detrending and original sequence.

defined as the area-averaged ON snow cover over eastern Europe and western Siberia (ES: 50–60° N, 40–90° E CE5). This domain was consistent with the centers of the dominant varied mode calculated by Sun (2017). The positive correla-

5 tion meant that if there was more SC_{ES}, then the haze pollution would be more severe over the CNC area. From the perspective of temporal variation, the SC_{ES} was more consistent with the DHD_{CNC} after the mid-1990s. Similar to the DHD_{CNC}, the maximum and minimum values of the SC_{ES}

10 were also observed in 2016 and 2010, respectively. It appeared that the correlation before the mid-1990s was not significant. Chronologically, the SC_{ES} decreased from 2000 to 2010, but it increased thereafter, which was similar to the DHD_{CNC}. Thus, the 21-year running correlation coefficient

15 (CC) between the DHD_{CNC} and SC_{ES} was calculated and plotted in Fig. 1a. Obviously, the CC was strengthened and

became significant after the mid-1990s, exceeding the 99 % confidence level. The CC between the DHD_{CNC} and SC_{ES} during the period of 1998–2016 (P2) was 0.62 after detrending, which was more significant than that during the period 20 of 1979–1997 (P1), i.e., only 0.07. The ON Eurasian snow cover correlated with the SC_{ES} was greater, and the CC was also larger during P2 (Fig. 2), indicating that the snow cover covaried more within the key areas and could influence the local and teleconnected climate more significantly. However, 25 during P1, the CC over the eastern part of the ES area was insignificant. The intensity of the interannual variations (i.e., expressed by the standard deviation in Fig. 2) in snow cover over the Tibetan Plateau and Mongolian Plateau were evident during both P1 and P2. The interannual variation in snow 30 cover over eastern Europe and western Siberia was larger during P2 than during P1, which was also revealed by empirical orthogonal function analysis (Figure omitted TS10). Furthermore, during P2, the snow cover with larger interannual variation was distributed widely and zonally; in contrast, 35 during P1, the significantly varied snow cover was meridionally instead of zonally distributed and was only located to the north of the Black Sea; thus, it could not have been telecon-
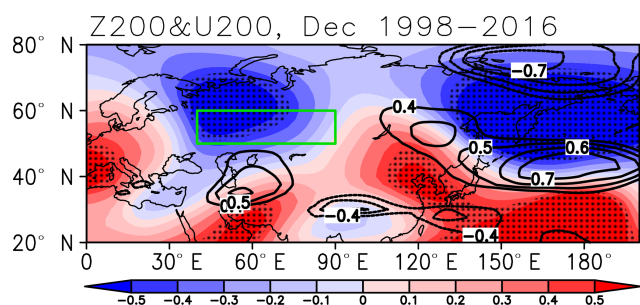
Figure 3. The CC between the SC_{ES} and Z200 (shading) and U200 (contour) in December from 1998 to 2016. The black dots indicate the CC exceeded the 95 % confidence level (t test). The green box represents the ES area. The linear trend is removed.
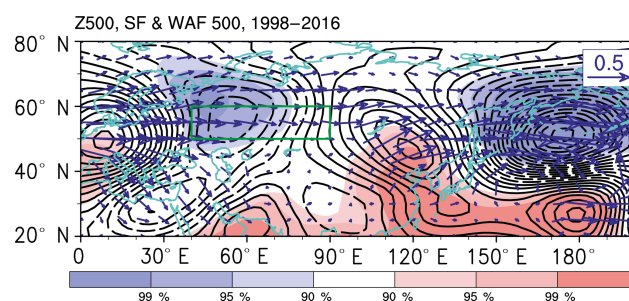
Figure 4. The CC between the SC_{ES} and Z500 (shading, exceeding 90, 95, and 99 % confidence levels), stream function (contour), and wave activity flux (arrow) in December from 1998 to 2016. The green box represents the ES area. The linear trend is removed.

nected with the haze pollution in China. We speculated that the varied interannual variation in the SC_{ES} possibly influenced the strengthening relationship shown in Fig. 1a. The impact of Arctic amplification on East Asian winter climate was significant (Wang and Liu, 2016; Zhou, 2017). Wang et al. (2015) illustrated that the decline in Arctic sea ice intensified the haze pollution in eastern China. Thus, we calculated the CC between the SC_{ES} (DHD_{CNC}) and the Arctic sea ice during P1 and P2, respectively. The SC_{ES} was insignificantly correlated with the September–November sea ice during P1 (Fig. S1 in the Supplement) but was significantly correlated with the ON sea ice over the Barents Sea (above 95 % confidence level) during P2 (Fig. S2). However, during P2, the CC between the ON sea ice over the Barents Sea and the DHD_{CNC} was not significant, indicating that the Eurasian snow cover was relatively independent of the Arctic sea ice in terms of its impact on haze pollution over the CNC area.

To explore the reasons for the observed strengthening relationship, the associated atmospheric circulations with the SC_{ES} during P2 are shown in Figs. 3–5. In the upper troposphere, the induced centers of atmospheric activities appeared as a "+−+−" pattern, including the positive centers located in western Europe, North China, and the Japan Sea and the negative centers over north of the Caspian Sea and the Aleutian Islands (Fig. 3). This Rossby wave-like pattern also existed and propagated with observed wave activity flux in the mid-troposphere (Fig. 4). The positive anomalies over North China and the Japan Sea were connected with the subtropical high in the Pacific, resulting in a strong pressure gradient in the south of the Aleutian Low CE6. The East Asia jet stream (EAJS), particularly its western end, was located more northward, meaning that the activities of the Rossby waves were also located more northward, and the cold air moving southward to the CNC area was weak (Chen and Wang, 2015). The associated vertical velocity at the surface was upward (Fig. 5a), indicating weak convergences of the aerosols discharged in the circumjacent regions. However, due to the shallower planetary boundary layer (Fig. 5a), the converging and local aerosols cannot be dispersed into the

upper atmosphere. The local convergences, combined with the weak surface wind (Fig. 5b), easily enabled aerosols to accumulate over the CNC area. Near the surface, the positive SLP anomalies were situated in the east of China and the western Pacific (Fig. 5c). The stimulated southerlies overlapped with the mean flow of the East Asian winter monsoon to weaken the cold northerly winds. The SAT of Eurasia was warmer, and the surface wind speeds over the CNC area were significantly reduced; thus, the horizontal ventilation capacity of the atmosphere over the CNC area was weak, and it was difficult for the air pollutants to disperse. Moreover, the enhanced water vapor transportation by the anomalous southerlies (Fig. 5b) provided a beneficial environment for hygroscopic growth, which is an important process for the formation of severe haze pollution. In summary, during P2, the atmospheric circulations and local meteorological conditions, which were related with the SC_{ES}, effectively confined the vertical and horizontal dispersion of atmospheric particles.

For comparison, the associated atmospheric circulations during P1 are shown in Figs. 6–8. In the high and mid-troposphere, the zonal Rossby wave-like pattern, which existed during P2, could not be identified; rather, another pattern propagated meridionally from the Mediterranean Sea to the polar region and then through Northeast China and the Sea of Okhotsk CE7 to the western Pacific (Figs. 6–7). The wide and zonal cyclonic anomalies located over Northeast China and the Sea of Okhotsk strengthened the EAJS and the meridional movement of cold air and resulted in the lower SAT in the east of China. The associated anomalous circulations tended to lead local meteorological conditions (e.g., higher BLH and more obvious surface wind speed) to favor ventilation (Fig. 8), which was consistent with the 21-year running CC in Fig. 1a (i.e., negative before the mid-1990s). However, this negative relationship was not significant because the correlated area of BLH and surface wind was too narrow; additionally, the surface vertical motion and relative humidity were not significantly correlated with the SC_{ES} during P1.
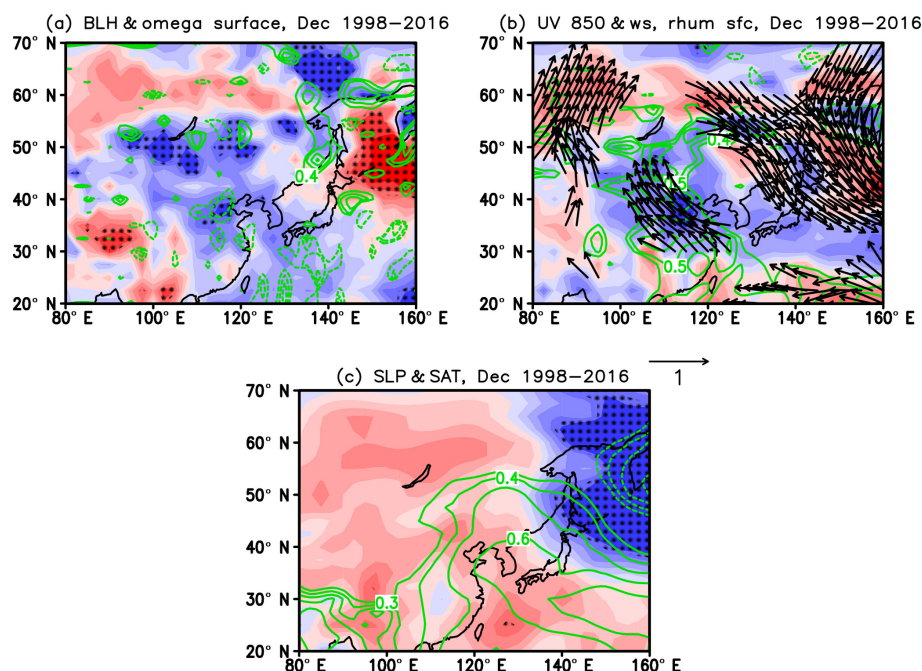
Figure 5. The CC between the SC$_{ES}$ and **(a)** BLH (shading) and surface omega (contour), **(b)** wind at 850 hPa (arrow), surface wind speed (shading), and surface relative humidity (contour), and **(c)** SLP (contour) and SAT (shading) in December from 1998 to 2016. The black dots indicate the CC exceeded the 95 % confidence level (t test). The linear trend is removed.
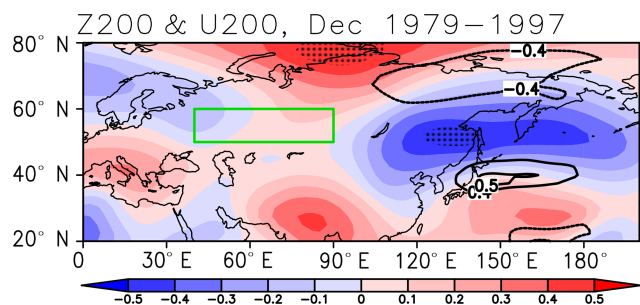
Figure 6. The CC between the SC$_{ES}$ and Z200 (shading) and U200 (contour) in December from 1979 to 1997. The black dots indicate the CC exceeded the 95 % confidence level (t test). The green box represents the ES area. The linear trend is removed.
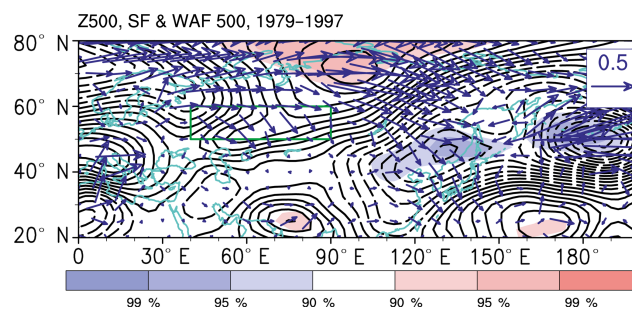
Figure 7. The CC between the SC$_{ES1}$ and Z500 (shading, exceeding 90, 95, and 99 % confidence levels), stream function (contour), and wave activity flux (arrow) in December from 1979 to 1997. The green box represents the ES area. The linear trend is removed.

4   Possible physical mechanisms

In autumn, the snowfall began in the mid-to-high CE8 latitudes. Because the SAT was not persistently below freezing point, part of the snow melted, and the soil moisture increased. In addition to the snow melt, the accumulated snow cover also reduced the moisture that evaporated from the land surface. During P2, the SC$_{ES}$ was significantly positively correlated with soil moisture around the Caspian Sea, Lake Balkhash CE9, and the Ural Mountains (Fig. 9, RM1: 40–60° N, 50–80° E). In addition, when the SC$_{ES}$ was greater, the soil was drier to the northeast of Lake Baikal (RM2: 52.5–62.5° N, 100–130° E) . These two significant correla-

tions persisted and were enhanced in December, i.e., the CC between the ON snow cover and the December soil moisture was larger than that between the ON snow cover and the ON soil moisture, both in the RM1 and RM2 areas. The area-averaged soil moisture in RM1 (RM2) was denoted as SoilM$_{RM1}$ (SoilM$_{RM2}$), and the SoilM index was defined as the difference between SoilM$_{RM1}$ and SoilM$_{RM2}$ (i.e., SoilM = SoilM$_{RM1}$−SoilM$_{RM2}$). During P2, the CC between the DHD$_{CNC}$ and the ON (December) SoilM index was 0.69 (0.69) after the removal of the linear trend, and it exceeded the 99 % confidence level; however, these significant correlations did not exist during P1 (Table 1). We speculated that the ON snow cover could impact the soil moisture in the RM1
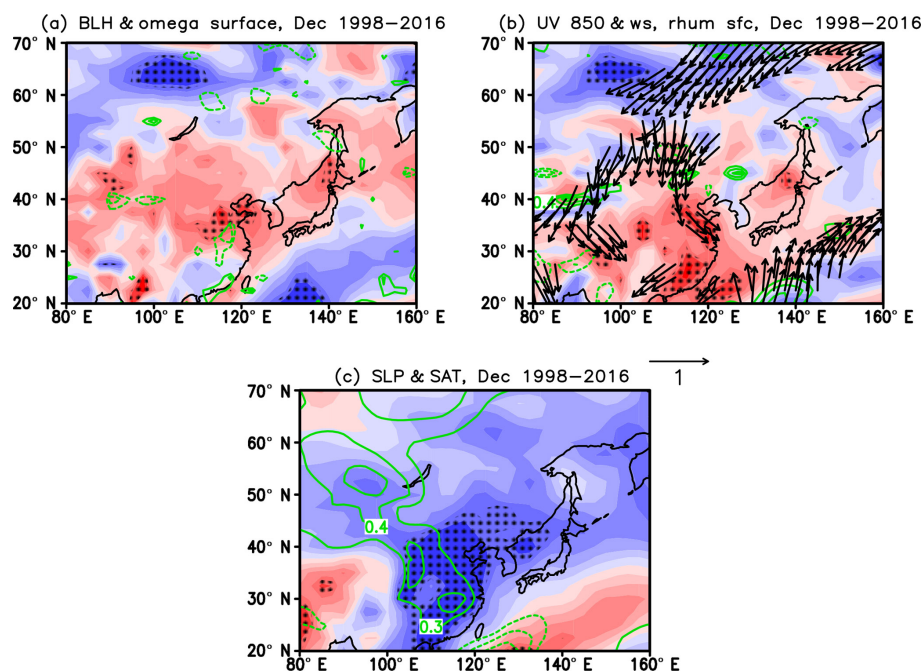
Figure 8. The CC between the SC_{ES1} and **(a)** BLH (shading) and surface omega (contour), **(b)** wind at 850 hPa (arrow), surface wind speed (shading), and surface relative humidity (contour), and **(c)** SLP (contour) and SAT (shading) in December from 1979 to 1997. The black dots indicate the CC exceeded the 95 % confidence level (t test). The linear trend is removed.
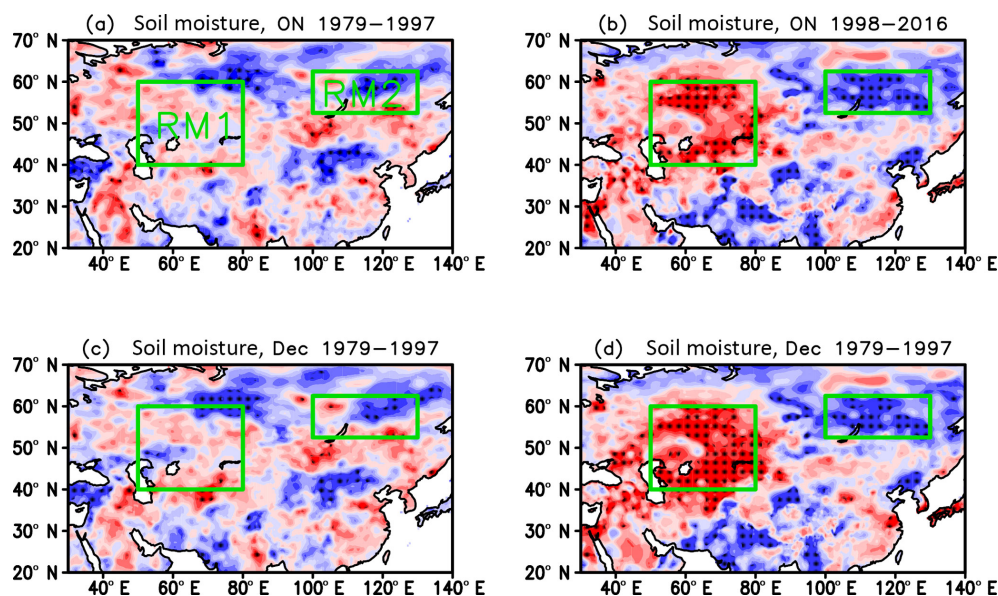
Figure 9. The CC between the SC_{ES} and soil moisture in **(a)** October–November (ON) and **(c)** December (Dec.) from 1979 to 1997, and in **(b)** October–November and **(d)** December from 1998 to 2016. The black dots indicate the CC exceeded the 95 % confidence level (t test). The linear trend is removed. The green boxes (RM1 and RM2) are the significantly correlated areas, which were used to calculate the SoilM index.
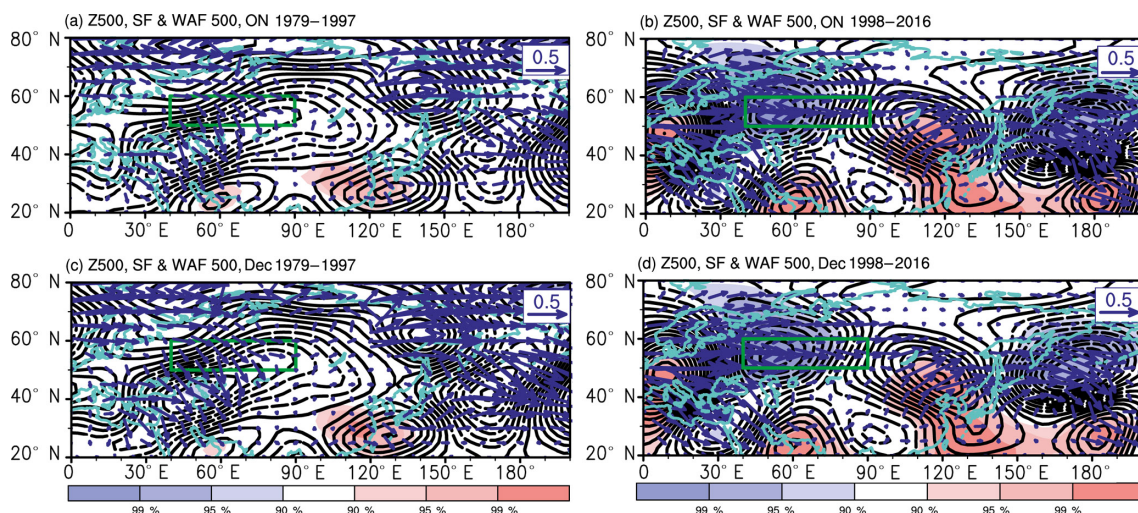
Figure 10. The CC between the SoilM index and Z500 (shading, exceeding 90, 95, and 99 % confidence levels), stream function (contour), and wave activity flux (arrow) in **(a)** October–November and **(c)** December from 1979 to 1997 and in **(b)** October–November and **(d)** December from 1998 to 2016. The green box represents the ES area. The linear trend is removed.

and RM2 areas, which could last into December, and then influence the December haze pollution through atmospheric circulations. Thus, the associated atmospheric circulations in the mid-troposphere were calculated and shown in Fig. 10. During P1, the impacts of the SoilM index on Z500 were not significant in ON or December, but this was consistent with the weak relationships between the SC_{ES} and DHD_{CNC}. In contrast, the significantly induced atmospheric circulations were distributed as a zonal Rossby wave pattern during P2 (Fig. 10b, d), which is similar to the data shown in Fig. 4. Particularly, the anomalous anti-cyclonic circulation over the CNC area was significant both in ON and December and was connected with the weak dispersion capacities of the atmospheric particles. The possible physical processes causing this could include the larger snow cover increasing the local soil moisture by melting and impeding evaporation, and the wetter land surface may have persisted and been enhanced in December. The "west wet-east dry" pattern of soil moisture could influence the atmospheric circulations, which would benefit the occurrence of haze pollution as a result of poor dispersion conditions. During P1, both the CC between the SC_{ES} and the SoilM index and the CC between the SoilM index and the DHD_{CNC} were not significant, indicating that the snow cover in the study area did not impact the DHD_{CNC} through effects on land surface moisture.

High albedo is another obvious characteristic of snow cover, which reflects more solar shortwave radiation and results in lower SAT. As a feedback, the outgoing longwave radiations emitted by the cooler land surface were weakened and had radiative cooling impacts on the atmosphere (Zhang et al., 2017). That is to say, the absorbed shortwave and outgoing longwave radiations were both reduced. As shown in Fig. 11, the correlated areas of radiation, including the loca-

Table 1. The CC between the DHD_{CNC} and SoilM index in October–November (ON) and December (Dec). OS means "original sequence" and "DT" means that the linear trend was removed.

CC	1979–1997		1998–2016	
	OS	DT	OS	DT
ON	0.15	0.14	0.77[b]	0.69[b]
Dec	0.13	−0.10	0.78[b]	0.69[b]

[a] indicates the result passed the 95 % confidence level, **TS12**
[b] indicates the CC passed the 99 % confidence level.

tion and shape, were apparently different during these two periods. During P1, the significant CCs between the SC_{ES} and net shortwave radiation were distributed from the southwest (i.e., Pamir Mountains) to the northeast (i.e., Sayan Mountains); this was denoted as RS1 (38–58° N, 70–100° E) and was mountainous (Fig. 11c). In contrast, the regions that had significant and negative CCs and net longwave radiation were smaller and over the Pamir Mountains (Fig. 11a; RL1: 36–45° N, 67.5–90° E). By contrast, the significant correlated regions with net longwave radiation (Fig. 11b; RL2) and net shortwave radiation (Fig. 11d; RS2) were the same and nearly overlapped with the ES area during P2, which was wider and had a zonal distribution. According to the above analysis, if there was more SC_{ES}, the net shortwave and net longwave radiations were both reduced, i.e., the absolute value of the net longwave radiation and net shortwave radiation would both be smaller. To assess the combined effects of radiation, the I_{LS} index was defined as the sum of the absolute value of the area-averaged net shortwave radiation ($|I_{RS}|$) and the absolute value of the area-averaged net longwave radiation ($|I_{RL}|$), i.e., $I_{LS1} = |I_{RL1}| + |I_{RS1}|$
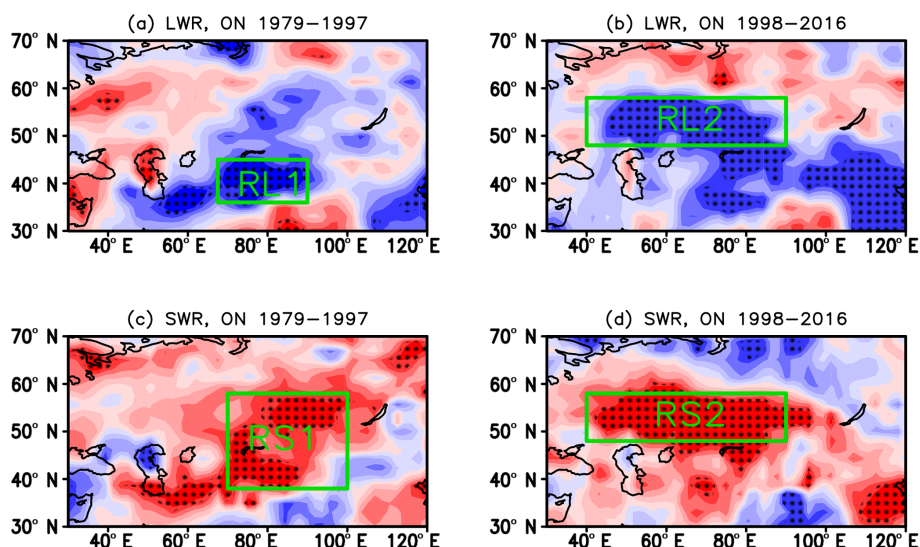
Figure 11. The CC between the SC_{ES} and **(a)** longwave radiation and **(c)** shortwave radiation in October–November from 1979 to 1997 and the CC between the SC_{ES} and **(b)** longwave radiation and **(c)** CE10 shortwave radiation in October–November from 1998 to 2016. The black dots indicate the CC exceeded the 95 % confidence level (*t* test). The linear trend is removed. The green boxes (RL and RS) are the significantly correlated areas, which were used to calculate the I_{LS1} (I_{LS2}).
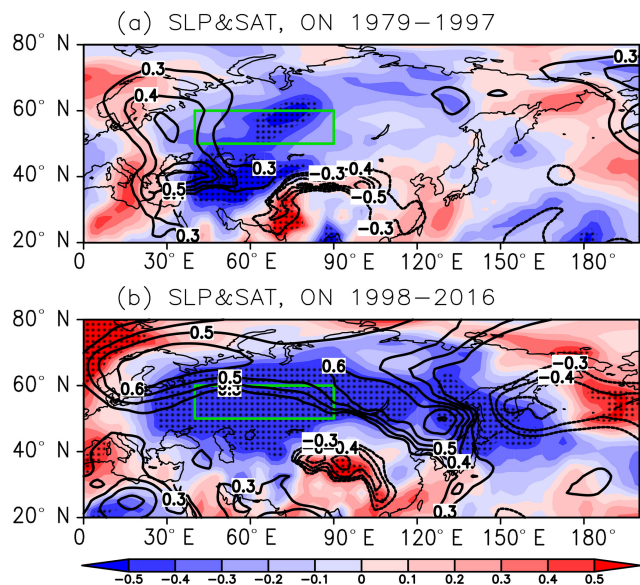
Figure 12. The CC between the SC_{ES} and SAT (shading) and SLP (contour) in October–November **(a)** from 1979 to 1997 and **(b)** from 1998 to 2016. The black dots indicate the CC exceeded the 95 % confidence level (*t* test). The green box represents the ES area. The linear trend is removed.

and $I_{LS2} = |I_{RL2}| + |I_{RS2}|$. It was obvious that when there was more snow cover, the I_{LS1} and I_{LS2} should be smaller. After removing the linear trend, the CCs between I_{LS} and DHD_{CNC} were calculated and were 0.07 (I_{LS1}, not significant) and -0.72 (I_{LS2}, above 99 % confidence level). We speculated that the ON snow cover would influence the De-

cember haze pollution by modulating the radiation during P2, but this process did not exist during P1. In fact, Cohen et al. (2007) noted that the diabatic cooling in late autumn, which was in accordance with the higher-than-normal snow cover, locally induced higher SLP anomalies and colder SAT; then, significant influences on the tropospheric atmosphere were observed the following winter through stratosphere–troposphere coupling. During P2, because of radiative cooling, the ON SAT was lower over the ES area and was zonally spread to the Sea of Okhotsk. Positive ON SLP anomalies were also stimulated in the mid-to-high latitudes of Eurasia. The induced SLP and SAT anomalies were zonal and almost occupied the mid-to-high latitudes of Eurasia. In contrast, the SLP and SAT anomalies during P1 were more meridional and smaller, and were more westward and located over Europe (Fig. 12). Consistent with the radiative drivers from the underlying surface (i.e., radiative cooling), during the following December, the atmospheric responses were more zonal during P2 but tended to be meridional during P1. Moreover, the atmospheric responses during P2 were stronger than those during P1 (Fig. 13). The induced Rossby wave pattern and anomalous EAJS during P2 (P1) were similar with those in Figs. 3 (6) and 4 (7). Because of the deep anti-cyclonic anomalies over North China and the subtropical western Pacific, the western end of EAJS was shifted significantly northward, resulting in weak cold air activities during the following December. In the mid-troposphere, there were Z500 anomaly centers located over western Europe (+), the area north of the Caspian Sea (−), North China and the Japan Sea (+), and the Aleutian Islands (−). The teleconnected pattern impacted the local meteorological conditions, such as a
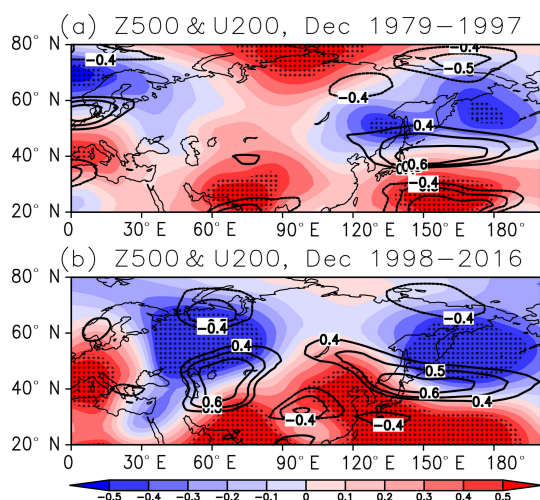
Figure 13. The CC between **(a)** I_{LS1}, **(b)** I_{LS2} and Z500 (shading) and U200 (contour) in December. The black dots indicate the CC exceeded the 95 % confidence level (t test). The linear trend is removed.

Table 2. The CC between the DHD$_{CNC}$ and I_{LS1} (I_{LS2}). OS means "original sequence", and "DT" means that the linear trend was removed. TS13

CC	1979–1997		1998–2016	
	OS	DT	OS	DT
I_{LS1}	-0.67^b	0.07	–	
I_{LS2}	–		-0.78^b	-0.72^b

[a] indicates the result passed the 95 % confidence level, TS14
[b] indicates the CC passed the 99 % confidence level.

shallower boundary layer, small surface wind speed, and sufficient water vapor, which confined the ventilation capacities of the air over the CNC area. The resulting pattern that appeared is shown in Fig. 7, and the pattern propagated through the Mediterranean Sea (+), northwest Europe (−), the polar region (+), Northeast China and the Sea of Okhotsk (−), and the western Pacific (+), and also existed in Fig. 13a. The subtropical high was located over the ocean, and the Aleutian Low extended westward to the CNC area. The EAJS was enhanced by the significant gradients, indicating obvious meridional cold air activity. Furthermore, there were no significant responses over the CNC area; thus, the impact on the local ventilation conditions were not obvious and resulted in a weak relationship with the occurrence of haze.

5 Conclusions and discussions

The haze pollution in December has become increasingly serious in the past decade (Fig. 1a), and the DHD$_{CNC}$ reached 21 days in 2016. Considering the evident damage of the increasing haze, it is meaningful to study the climatic factors that are closely related to haze in China. Yin and Wang (2017) illustrated that the snow cover over eastern Europe and western Siberia influenced the DHD$_{CNC}$ from 1979 to 2016, but they did not give adequate attention to the physical mechanisms. In this study, we found that the relationship between the SC$_{ES}$ and DHD$_{CNC}$ also varied and was strengthened after the mid-1990s. During 1998–2016, the interannual variation in the SC$_{ES}$ was more significant, and the snow cover with larger interannual variation was distributed zonally and occupied the entirety of eastern Europe and western Siberia; thus, the forcing effects were more effective than those during 1979–1997. The associated soil moisture (partially indicating the water effect) and radiation (related with high albedo) were significantly different during these two periods. The radiative cooling effects of the SC$_{ES}$ during the later period were significant and overlapped with the whole target area of snow cover, which was more zonal, broader, and stronger than those in the period of 1979–1997. The soil moisture was also significantly correlated with the SC$_{ES}$, which could last to December between 1998 and 2016. In contrast, there was no close relationship between the Eurasian soil moisture and the SC$_{ES}$ from 1979 to 1997. Thus, during 1998–2016, the combined influences of the enhanced soil moisture and the radiative cooling that resulted from the positive SC$_{ES}$ anomalies could cause EAJS to shift northward and stimulate the anti-cyclonic anomalies over the CNC area. Under such atmospheric circulations, the local boundary layer was shallower, the surface wind speed was smaller, and the surface moisture was greater. As a result, the atmospheric particles accumulated easily, and the haze occurred frequently. During 1979–1997, both the linkage between the SC$_{ES}$ and soil moisture and the impacts of soil moisture on atmospheric circulations were negligible. The radiative cooling was the way in which the SC$_{ES}$ modulated the atmospheric circulations. Nevertheless, the correlated regions of radiation were smaller and meridional, and the resulting atmospheric circulations were not significantly linked to the ventilation conditions. Consequently, the relationship between the SC$_{ES}$ and DHD$_{CNC}$ was insignificant from 1979 to 1997 but was strengthened and became significant after the mid-1990s. To exemplify the associated mechanisms during 1998–2016, a diagram was drawn and supplemented as Fig. S3.

In this study, the varied relationship between the SC$_{ES}$ and DHD$_{CNC}$ and the associated physical mechanisms were analyzed, but more detailed investigations, such as the internal processes driving how the soil moisture (radiative cooling) impacted the atmosphere in the following December, were not included in this study and should be conducted with numerical models in future work. Many climatic factors at mid-to-high latitudes have been documented as effective external drivers, including Arctic sea ice (Wang et al., 2015, 2016), Eurasian SAT (Yin et al., 2017), SST in the Pacific (Yin and Wang, 2017), and Eurasian snow cover (Yin and Wang, 2017). Some questions raised here include why so many link-

ages are found in the mid-to-high latitudes and how they work together to impact the haze pollution in China. This is still an open question that needs to be answered. Another question that deserves more attention is why the relationship shifted in approximately 1998. One of the reasonable speculations is the impact of the Pacific Decadal Oscillation, whose phase also shifted in approximately 1998 CE11. The questions mentioned above will be addressed in our future work. As a result of the recent enhancement, the significant relationship possibly improved the potential to predict haze pollution, which is valuable for scientific decision-making related to controlling haze pollution in China.

Data availability. . TS15

The Supplement related to this article is available online at https://doi.org/10.5194/acp-18-1-2018-supplement.

Competing interests. The authors declare that they have no conflict of interest. TS16

Acknowledgements. This research was supported by the National Natural Science Foundation of China (41705058 and 91744311), the KLME Open Foundation (KLME1607), the CAS–PKU Partnership Program, the Startup Foundation for Introducing Talent of Nanjing University of Information Science and Technology (20172007), the funding of Jiangsu innovation & entrepreneurship team, and the Priority Academic Program Development (PAPD) of Jiangsu Higher Education Institutions.

Edited by: Aijun Ding
Reviewed by: two anonymous referees

References

Cai, W. J., Li, K., Liao, H., Wang, H. J., and Wu, L. X.: Weather Conditions Conducive to Beijing Severe Haze More Frequent under Climate Change, Nature Climate Change, TS17, https://doi.org/10.1038/nclimate3249, 2017.

Chen, H. P. and Wang, H. J.: Haze days in North China and the associated atmospheric circulations based on daily visibility data from 1960 to 2012, J. Geophys. Res.-Atmos., 120, 5895–5909, https://doi.org/10.1002/2015JD023225, 2015.

Cohen, J., Barlow, M., Kushner, P. J., and Saito, K.: Stratosphere and troposphere coupling and links with Eurasian land surface variability, J Climate, 20, 5335–5343, 2007.

Cohen, J. L., Furtado, J. C., Barlow, M. A., Alexeev, V. A., and Cherry, J. E.: Arctic warming, increasing snow cover and widespread boreal winter cooling, Environ. Res. Lett., 7, 014007, TS18, 2012.

Dee, D. P., Uppala, S. M., Simmons, A. J., Berrisford, P., Poli, P., Kobayashi, S., Andrae, U., Balmaseda, M. A., Balsamo, G., Bauer, P., Bechtold, P., and Beljaars, A. C. M.: The ERA-Interim reanalysis: configuration and performance of the data assimilation system, Q. J. Roy. Meteor. Soc., 137, 553–597, https://doi.org/10.1002/qj.828, 2011.

Deser, C., Tomas, R., Alexander, M., and Lawrence, D.: The seasonal atmospheric response to projected Arctic sea ice loss in the late twentyfirst century, J. Clim., 23, 333–351, https://doi.org/10.1175/2009JCLI3053.1, 2010.

Ding, A. J., Huang, X., Nie, W., Sun, J. N., Kerminen, V. M., Petäjä, T., Su, H., Cheng, Y. F., Yang, X. Q., Wang, M. H., et al. TS19: Enhanced haze pollution by black carbon in megacities in China, Geophys. Res. Lett., 43, 2873–2879, https://doi.org/10.1002/2016GL067745, 2016.

Ding, Y. H. and Liu, Y. J.: Analysis of long-term variations of fog and haze in China in recent 50 years and their relations with atmospheric humidity, Sci. China Ser. D: Earth Sci., 57, 36–46, 2014 (in Chinese).

Foster, J., Owe, M., and Rango, A.: Snow cover and temperature relationships in North America and Eurasia, J. Appl. Meteorol., 22, 460–469, 1983.

Gao, Y. and Chen, D.: A dark October in Beijing 2016, Atmos. Oceanic Sci. Lett., 10, 206–213, 2017.

Gao, H. and Li, X.: Influences of El Nino Southern Oscillation events on haze frequency in eastern China during boreal winters, Int. J. Climatol., 35, TS20, https://doi.org/10.1002/joc.4133, 2015. TS21

Gong, G., Cohen, J., Entekhabi, D., and Ge, Y.: Hemispheric-scale climate response to Northern Eurasia land surface characteristics and snow anomalies, Global Planet Change, 56, 359–370, 2007.

Jeong, J. H., Ou, T., Linderholm, H. W., Kim, B. M., Kim, S. J., Kug, J. S., and Chen, D. L.: Recent recovery of the siberian high intensity, J. Geophys. Res.-Atmos., 116, D23102, TS22, 2011.

Kalnay, E., Kanamitsu, M., Kistler, R., Collins, W., Deaven, D., Gandin, L., Iredell, M., Saha, S., White, G., Woollen, J., Zhu, Y., Leetmaa, A., Reynolds, R., Chelliah, M., Ebisuzaki, W., Higgins, W., Janowiak, J., Mo, K. C., Ropelewski, C., Wang, J., Jenne, R., and Joseph, D.: The NCEP/NCAR 40-year reanalysis project, B. Am. Meteorol. Soc., 77, 437–471, https://doi.org/10.1175/1520-0477(1996)077<0437:TNYRP>2.0.CO;2, 1996.

Li, F. and Wang, H. J.: Autumn Eurasian snow depth, autumn Arctic sea ice cover and East Asian winter monsoon, Int. J. Climatol., 34, 3616–3625, 2014.

Li, H., Wang, H., and Jiang, D.: Influence of October Eurasian snow on winter temperature over Northeast China, Adv Atmos Sci., TS23, https://doi.org/10.1007/s00376-016-5274-0, 2017.

Li, Q., Zhang, R. H., and Wang, Y.: Interannual variation of the winter-time fog–haze days across central and eastern China and its relation with East Asian winter monsoon, Int. J. Climatol., 36, 346–354, https://doi.org/10.1002/joc.4350, 2015.

Robinson, D. A., Dewey, K. F., and Heim Jr., R.: Global snow cover monitoring: an update, B. Am. Meteorol. Soc., 74, 1689–1696, 1993.

Sun, B. TS24: Seasonal evolution of the dominant modes of the Eurasian snowpack and atmospheric circulation from autumn to the subsequent spring and the associated surface heat budget, Atmos. Oceanic Sci. Lett., 10, 191–197, https://doi.org/10.1080/16742834.2017.1286226, 2017.

Wang, H.-J. and Chen, H.-P.: Understanding the recent trend of haze pollution in eastern China: roles of climate change, Atmos. Chem. Phys., 16, 4205–4211, https://doi.org/10.5194/acp-16-4205-2016, 2016.

Wang, H. J., Chen, H. P., and Liu, J. P.: Arctic sea ice decline intensified haze pollution in eastern China, Atmos. Oceanic Sci. Lett., 8, 1–9, 2015.

Wang, S. Y. and Liu, J. P.: Delving into the relationship between autumn Arctic sea ice and central–eastern Eurasian winter climate, Atmos. Oceanic Sci. Lett., 9, 366–374, https://doi.org/10.1080/16742834.2016.1207482, 2016.

Xu, X., Zhao, T., Liu, F., Gong, S. L., Kristovich, D., Lu, C., Guo, Y., Cheng, X., Wang, Y., and Ding, G.: Climate modulation of the Tibetan Plateau on haze in China, Atmos. Chem. Phys., 16, 1365–1375, https://doi.org/10.5194/acp-16-1365-2016, 2016.

Xu, X. P., He, S. P., Li, F., and Wang, H. J.: Impact of northern eurasian snow cover in autumn on the warm arctic–cold eurasia pattern during the following january and its linkage to stationary planetary waves, Clim. Dynam., TS25, 1–14, https://doi.org/10.1007/s00382-017-3732-8, 2017.

Yang, T., Sun, Y., Zhang, W., Wang, Z., and Wang, X. TS26: Chemical characterization of submicron particles during typical air pollution episodes in spring over Beijing, Atmos. Oceanic Sci. Lett., 9, 255–262, https://doi.org/10.1080/16742834.2016.1173509, 2016.

Yang, Y., Liao, H., and Lou, S.: Increase in winter haze over eastern China in recent decades: Roles of variations in meteorological parameters and anthropogenic emissions, J. Geophys. Res.-Atmos., 121, 13050–13065, 2016.

Yang, Y., Russell, L. M., Lou, S., Liao, H., Guo, J., Liu, Y., Singh, B., and Ghan, S. J.: Dustwind interactions can intensify aerosol pollution over eastern China, Nat. Commun., 8, 15333, https://doi.org/10.1038/ncomms15333, 2017a.

Yang, Y., Wang, H., Smith, S. J., Ma, P.-L., and Rasch, P. J.: Source attribution of black carbon and its direct radiative forcing in China, Atmos. Chem. Phys., 17, 4319–4336, https://doi.org/10.5194/acp-17-4319-2017, 2017b.

Yin, Z. and Wang, H.: Role of atmospheric circulations in haze pollution in December 2016, Atmos. Chem. Phys., 17, 11673–11681, https://doi.org/10.5194/acp-17-11673-2017, 2017.

Yin, Z., Wang, H., and Chen, H.: Understanding severe winter haze events in the North China Plain in 2014: roles of climate anomalies, Atmos. Chem. Phys., 17, 1641–1651, https://doi.org/10.5194/acp-17-1641-2017, 2017.

Yin, Z. C. and Wang, H. J.: The relationship between the subtropical Western Pacific SST and haze over North-Central North China Plain, Int. J. Climatol., 36, 3479–3491, https://doi.org/10.1002/joc.4570, 2016.

Yin, Z. C., Wang, H. J., and Yuan, D. M.: Interdecadal increase of haze in winter over North China and the Huang-huai area and the weakening of the East Asia winter monsoon, Chin. Sci. Bull., 60, 1395–1400, 2015 (in Chinese).

Yuan, D. M. and Ma, X. H.: The severe haze in 16–21 December 2016 and associated atmospheric circulation anomalies, Climatic and Environmental Research, accepted TS27, 2017 (in Chinese).

Zhang, F., Yan, J. R., Li, J. N., Wu, K., Iwabuchi, H., and Shi, Y. N.: A new radiative transfer method for solar radiation in a vertically internally inhomogeneous medium, J. Atmos. Sci., TS28, https://doi.org/10.1175/JAS-D-17-0104.1, 2017,

Zhang, T. Y., Chen, H. H., and Sun, Z. B.: The Relationship between Autumn-time Eurasian Snow Cover and Winter-time NH Circulation, Acta Geographica Sinica, 62, 728–741, 2007.

Zhou, W. TS29: Impact of Arctic amplification on East Asian winter climate, Atmos. Oceanic Sci. Lett., 10, 385–388, https://doi.org/10.1080/16742834.2017.1350093, 2017.

Zou, Y. F., Wang, Y. H., Zhang, Y. Z., and Koo, J. H.: Arctic sea ice, Eurasia snow, and extreme winter haze in China, Science Advances, 3, e1602751, https://doi.org/10.1126/sciadv.1602751, 2017.

Remarks from the language copy-editor

Remarks from the typesetter

TS15 Please provide a statement on how your underlying research data can be accessed. If the data are not publicly accessible, a detailed explanation of why this is the case is required. The best way to provide access to data is by depositing them (as well as related metadata) in reliable public data repositories, assigning digital object identifiers (DOIs), and properly citing data sets as individual contributions. Please indicate if different data sets are deposited in different repositories or if data from a third party were used. If no DOI is available, assets can be linked through persistent URLs to the data set itself (not to the repositories' home page). This is not seen as best practice and the persistence of the URL must be secured.

TS29 Please confirm.